physica status solidi pss a
www.pss-a.com

Emerging Applications of III-Nitride Nanocrystals

*Xianhe Liu, Faqrul A. Chowdhury, Srinivas Vanka, Sheng Chu, and Zetian Mi**

Recently, significant progress has been made in III-nitride nanocrystals. They exhibit unique structural, electronic, optical, and photocatalytic properties, and have emerged as a functional platform to realize high-performance optoelectronic, electronic, quantum, and solar energy devices. Compared with conventional III-nitride epilayers and quantum wells, dislocation-free III-nitride nanocrystals can, in principle, be achieved on lattice mismatched foreign substrates due to the efficient surface strain relaxation. In this Feature Article, the authors discuss the epitaxy, characteristics, and some emerging device applications of III-nitride nanocrystals grown by plasma-assisted molecular beam epitaxy.

1. Introduction

In the past decades, we have witnessed the tremendous success of GaN semiconductors. Through the pioneering work of Akasaki, Amano, and Nakamura and many others, GaN is the material of choice for today's massive light emitting diode (LED) lighting industry.[1–3] It has also emerged as the next-generation power semiconductor.[4,5] Despite the great success, however, there are many critical challenges that remain to be addressed. For example, GaN-based LEDs still exhibit low efficiency in the green and red wavelengths.[6] In the deep ultraviolet (UV) spectrum, the efficiency of AlGaN-based LEDs is well below 10%.[7–9] Although significant progress has been made in optically pumped AlGaN quantum well laser diodes in the mid and deep UV spectra, there has been only one report of electrically pumped quantum well laser diodes operating in the UV-B and UV-C bands. In addition, there is an urgent need to develop multicolor micro-LEDs to improve the efficiency of mobile displays. Such small size LED arrays are also essentially required for the emerging virtual/augmented/mixed reality devices and systems. It is further envisioned that III-nitrides can play a critical role in addressing the critical energy and environmental challenges we face in the 21st century. The energy bandgap of InGaN can be tuned across nearly the entire solar spectrum. Recent studies have further shown that InGaN is the only known semiconductor whose conduction and valence band edges can straddle water redox potentials under deep visible and near infrared light irradiation, which is essentially required for the efficient generation of solar fuels through solar water splitting and CO_2 reduction.[10–12]

One major challenge to realize these promises is the presence of extensive defects and dislocations in the epitaxy of III-nitride heterostructures. In this regard, tremendous success has been made in the development and commercialization of GaN and AlN substrates/templates. Studies by Miyake at Mie University showed that the quality of AlN grown/deposited on sapphire wafer can be substantially improved by ultrahigh temperature annealing.[13–15] High-quality AlN has also been demonstrated by growing on nano-patterned sapphire wafer.[16–19] Due to the efficient strain relaxation, dislocation-free III-nitride nanocrystals can, in principle, be achieved on foreign substrates.[20–30] Such nanostructures were first developed in the 1990s by Kishino and Calleja.[31–33] Since then, III-nitride nanocrystals, also commonly referred to as nanowires, or nanorods, have been intensively studied.[21,34–44] They have emerged as unique platform, not only for materials studies but also for many practical device applications, including LEDs, lasers, photodetectors, transistors, solar cells, and artificial photosynthesis, to name just a few.

In this article, we provide an overview on some of the emerging applications of III-nitride nanocrystals. In Section 2, we describe the realization of nearly dislocation-free AlGaN templates through controlled coalescence of III-nitride nanocrystals. The unique epitaxy of III-nitride nanocrystals and the realization of multi-color nano/micro-LEDs is presented in Section 3. In Section 4, we present the recent demonstration of surface-emitting green laser diodes with the use of III-nitride nanocrystal arrays. The achievement of efficient p-type conduction of AlN nanocrystals, and the realization of mid and deep UV LEDs and laser diodes is discussed in Section 5. In Section 6, the unique advantages of InGaN nanocrystals for solar fuel production and the recent developments in GaN-based artificial photosynthesis are described. Finally, conclusions and future prospects are discussed in Section 7.

Dr. X. Liu, Dr. S. Vanka, Prof. Z. Mi
Department of Electrical Engineering and Computer Science
University of Michigan
Ann Arbor, MI 48109, USA
E-mail: ztmi@umich.edu

Dr. X. Liu, Dr. F. A. Chowdhury
Department of Physics
McGill University
Montreal, Quebec H3A 2T8, Canada

Dr. S. Chu
Department of Electrical and Computer Engineering
McGill University
Montreal, Quebec H3A 0E9, Canada

The ORCID identification number(s) for the author(s) of this article can be found under https://doi.org/10.1002/pssa.201900885.

DOI: 10.1002/pssa.201900885

2. Dislocation-Free AlGaN Templates through Controlled Coalescence of Nanocrystals

Given that dislocation-free nanocrystals can be grown directly on foreign substrates due to the efficient surface strain relaxation, the coalescence of nanocrystals has been studied for forming high-quality templates on foreign substrates.[45–47] However, the presence of any mismatch between the crystal orientations at the coalescence boundary can lead to dislocations during the coalescence process.[48] **Figure 1**a schematically illustrates the generation of strain, grain boundaries, networks of structural defects upon the coalescence of two randomly oriented crystal structures.[47,49–51] Such issues can be potentially addressed if the two crystals have identical orientations at the coalescence boundary, as shown in Figure 1b. The formation of dislocations can, in principle, be eliminated due to the identical crystalline orientation. A small distortion in the lattice due to variation in bond length or angle can also be accommodated. Moreover, the controlled coalescence allows strain to be gradually relaxed to the bulk state, which also minimizes the generation of dislocations at coalescence boundaries. It is therefore expected that dislocation-free AlGaN template with arbitrary alloy compositions can be realized on foreign substrates.

Key to this process is control over the nucleation of nanocrystals to achieve identical crystalline orientation, crystal dimension, and well-defined position. In this regard, selective area epitaxy was used to form a highly regular AlGaN nanocrystal array. As shown in **Figure 2**a, a thin Ti layer was first deposited on a GaN-on-sapphire substrate to serve as the growth mask. Opening apertures were defined on the Ti layer using electron beam lithography and dry etching. Under optimized growth conditions, GaN nanocrystals were only formed in the opening apertures. The resulting GaN nanocrystals have a hexagonal morphology. AlGaN nanocrystals were subsequently grown on top. Due to the slower surface migration of Al adatoms than Ga adatoms, the lateral growth of nanocrystals was enhanced. As the growth proceeded, the nanocrystals gradually coalesced and a continuous AlGaN epilayer was formed on top, as shown in Figure 2b. The morphology of the AlGaN film exhibits semi-polar planes which stem from the semi-polar planes of the pyramid top of Ga-polar nanocrystals. The resulting semi-polar AlGaN template has several benefits, including reduced polarization field and enhanced p-type Mg-dopant incorporation.[52,53] Detailed studies showed that there were no dislocations or stacking faults at the coalescence boundary as shown in Figure 2c. The absence of structural defects is also attributed to the efficient strain relaxation in the quasi-3D structures of the well-ordered semi-polar surface.[23,54,55] The Al content of the AlGaN film was estimated to be ≈30%. Further characterization of the p-type conduction in the p-AlGaN film formed in this approach indicates a hole mobility of 8.85 $cm^2 V^{-1} s^{-1}$ and a hole concentration of 7.4×10^{18} cm^{-3} at room-temperature.[48] Compared with previously reported values for p-AlGaN with similar Al-content, the hole mobility is enhanced by a factor of two and the hole concentration is enhanced by more than one order of magnitude.[56–58] The activation energy for Mg-dopant is estimated to be ≈47 meV from detailed temperature-dependent Hall effect measurement, which is attributed to hopping conduction in the Mg-impurity band.[58,59]

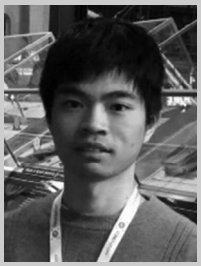

Xianhe Liu is a postdoctoral research associate in Prof. Zetian Mi's lab in the Department of Electrical Engineering and Computer Science. He obtained his Ph.D. degree from McGill University, Canada in 2019. His research interests are focused on the molecular beam epitaxial growth of III-nitride nanostructures with unique optical and electrical properties and the application of such nanostructures for enhancing the efficiency of optoelectronic devices including UV LEDs and lasers, and micro-LEDs. He is also interested in the simulation of optoelectronic devices based on these nanostructures.

Faqrul Chowdhury is a postdoctoral researcher at the Department of Physics, McGill University, Canada, who completed his Ph.D. in Electrical and Computer Engineering from the same institution as a Vanier Canada Graduate Scholar. He examines to understand and overcome the complexities and bottlenecks associated with artificial photosynthesis processes and systems. In the recent years, he has extensively worked on the systematic development of GaN-based efficient and stable artificial photosynthesis devices and their large-scale deployment. In broader perspective, his research interests center around novel III-nitride alloys and nanostructures for optoelectronics and solar fuels, molecular beam epitaxy, and heterogenous catalysis.

Zetian Mi is a Professor in the Department of Electrical Engineering and Computer Science at the University of Michigan, Ann Arbor. His teaching and research interests are in the areas of III-nitride semiconductors, LEDs, lasers, quantum photonics, solar fuels, and artificial photosynthesis.

3. Multi-Color Micro-LEDs

InGaN nanocrystals grown by molecular beam epitaxy (MBE) is well suited for realizing multi-color light emitters in a single growth process. As shown in **Figure 3**, the In content of InGaN nanocrystals is determined not only by directly impingent In atoms from the top surface but also on the supply of In adatoms through lateral surface migration. Consequently,

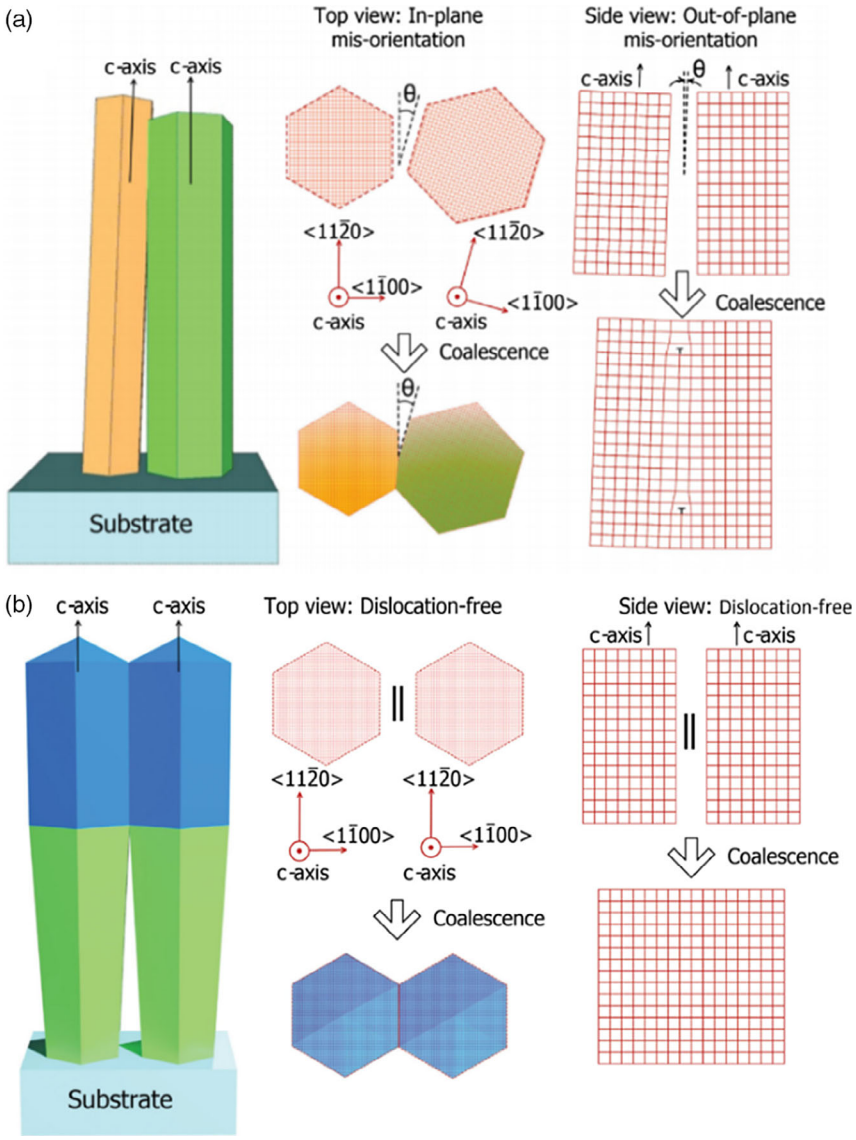

Figure 1. Schematics for the coalescence of nanocrystals with a) different orientations and b) identical orientation. Dislocations are expected at the boundary of coalescence in (a) but not in (b). The lattice is represented by simple cubic structure. Reproduced with permission.[48] Copyright 2016, Wiley-VCH Verlag GmbH & Co. KGaA.

the In content can be varied by changing the size of InGaN nanocrystals in a single growth step. As shown in **Figure 4**a, emission colors varying from blue to red can be achieved from nanocrystals of different sizes arranged in a triangular lattice.[61] The emission wavelengths redshifted from ≈480 to ≈630 nm with diameters increasing from 143 to 270 nm while keeping the period of the nanocrystal array constant, which corresponds to In content variation from 23% to 35%. By keeping the period constant, the spacing between nanocrystals is reduced with increasing diameter, leading to enhanced shadowing effect for adatoms on the sidewalls. Due to the shorter migration length of In adatoms compared with that of Ga adatoms at elevated growth temperature, the supply of Ga through lateral surface migration was more affected than that of In. As a result, the Ga incorporation became less for nanocrystals with smaller spacing, which caused redshifts in emission wavelengths for nanocrystals with larger diameters. Using this approach, multicolor micro-LEDs were demonstrated. Shown in Figure 4b are the electroluminescence (EL) spectra for monolithically integrated four micro-LEDs with different colors from blue to red.[62]

Control over emission wavelengths at the single nanocrystal level was also studied.[60] It was observed that the formation and properties of InGaN quantum dots (QDs) depend critically on the size of nanocrystals. As shown in **Figure 5**a, for GaN nanocrystals with relatively small size, InGaN QDs were incorporated at the center of the crystal. With increasing crystal size, InGaN QDs were formed on the semipolar planes near the lateral surfaces, shown in Figure 5b–d. This was explained by the enhanced indium incorporation near the center region for nanocrystals with smaller sizes, due to relatively large contribution

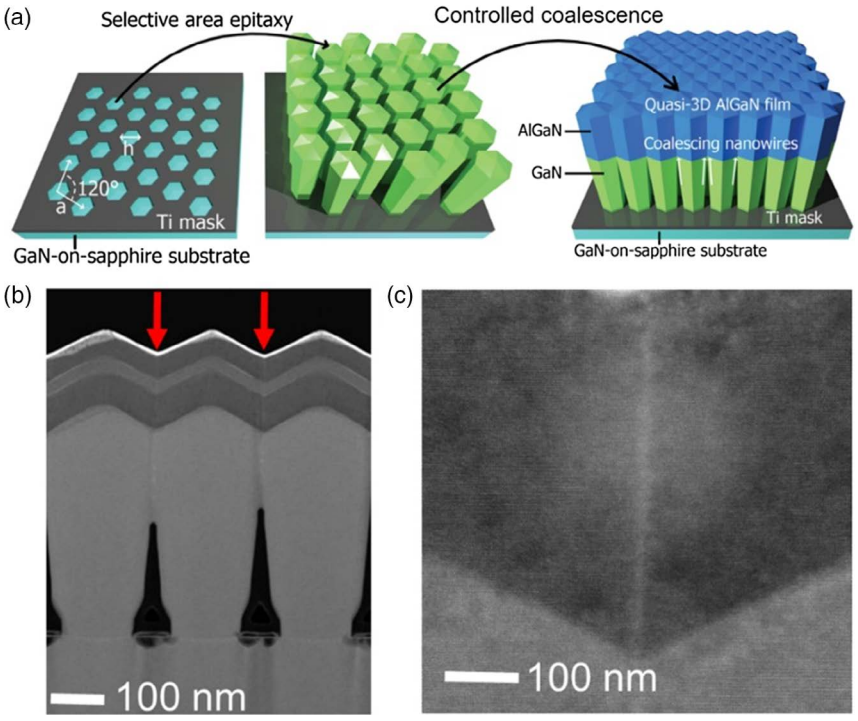

Figure 2. a) Schematic for the patterning preparation and selective area epitaxy of Ga(Al)N nanocrystals. b) Scanning transmission electron microscopy high-angle annular dark-field (STEM-HAADF) image of the cross section of a few nanocrystals. The red arrows indicate the boundary of coalescence. c) A high-magnification view of the boundary of coalescence showing the absence of structural defects. Reproduced with permission.[48] Copyright 2016, Wiley-VCH Verlag GmbH & Co. KGaA.

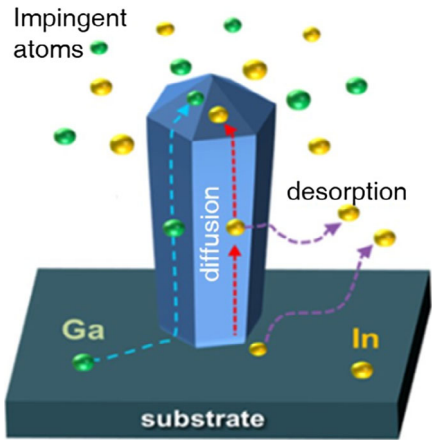

Figure 3. Schematic for the surface dynamics of In and Ga adatoms during the growth of InGaN nanocrystals. Reproduced with permission.[60] Copyright 2016, American Chemical Society.

from indium adatom migration on the lateral surfaces, compared with nanocrystals with larger sizes. Figure 5e shows the photoluminescence (PL) spectra measured for single InGaN nanocrystals with different diameters grown on the same substrate. It is seen that the emission wavelengths can be controllably varied from red to blue with increasing nanocrystal size. Detailed structural characterization further revealed that, during single nanocrystal epitaxy, indium incorporation is significantly enhanced for nanocrystals with smaller sizes, due to the enhanced indium incorporation from the lateral surfaces. Multi-color single nanocrystal LEDs were also fabricated and characterized,[60] which provide distinct opportunities to realize monolithically integrated red-green-blue micro and nano LED arrays.

By using selective area epitaxy, InGaN nanocrystals can be arranged to form a photonic crystal structure to enhance the radiative recombination rate by Purcell effect and to enhance the light extraction efficiency by Bragg scattering. **Figure 6**a shows the SEM image of a nanocrystal array designed to match the band edge Γ point with the emission wavelength.[63] At the band edge, the group velocity is drastically reduced, leading to a stable large area mode in the entire array and longtime interaction between the mode and the active region. Therefore, the Purcell effect can significantly enhance the radiative recombination rate and improve the internal quantum efficiency (IQE).[64] The resultant PL spectrum is shown in Figure 6b where a pronounced peak with a narrow linewidth of ≈12 nm is observed from the photonic crystal structure. The structure without photonic crystal resonance effect only exhibits a broad emission peak depicted by the blue curve in Figure 6b. Due to the emission property of photonic crystal, the emission spectrum remains extremely stable under a wide range of excitation powers from 29 W cm^{-2} to 17.5 kW cm^{-2}, as shown in Figure 6c. In contrast, the emission from conventional InGaN quantum wells usually blueshifts due to quantum Stark effect as the excitation power increases.[65,66] The analysis in Figure 6d shows negligible peak shift or broadening as the excitation power is varied by nearly

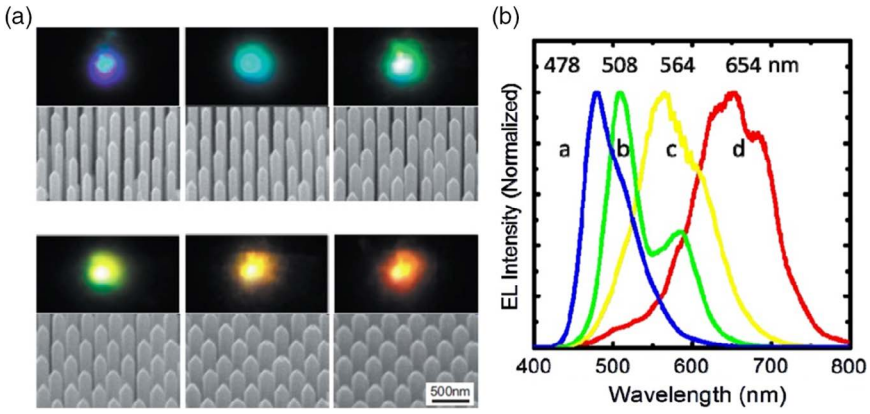

Figure 4. a) Scanning electron microscopy (SEM) images and photos for nanocrystal arrays with different diameters. Reproduced with permission.[61] Copyright 2010, American Institute of Physics. b) EL spectra for LEDs with different colors. Reproduced with permission.[62] Copyright 2017, Institute of Electrical and Electronics Engineers.

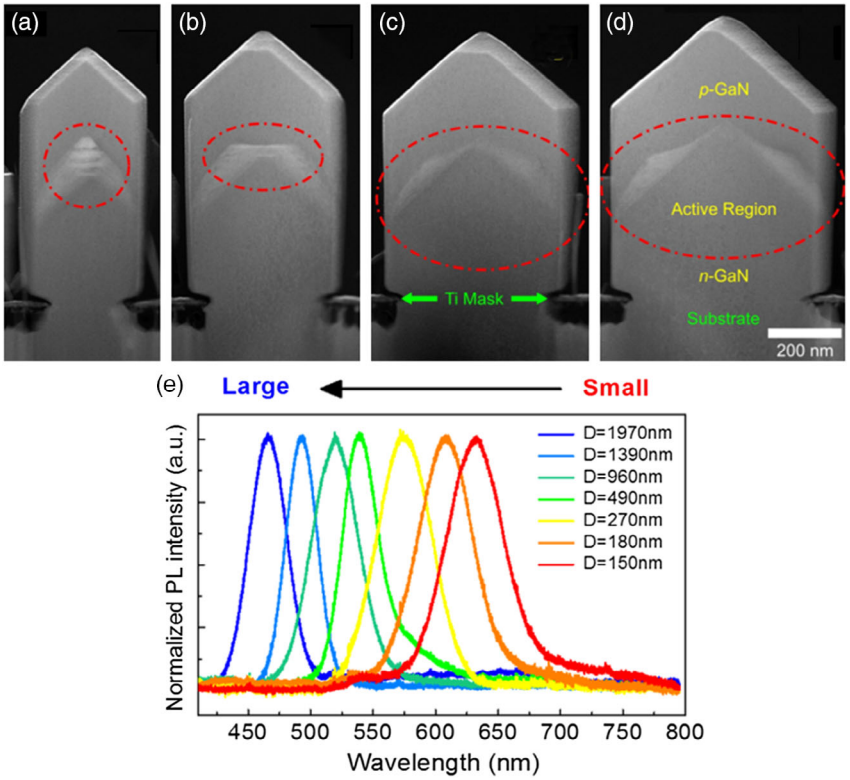

Figure 5. a–d) STEM-HAADF images for single nanocrystals with different diameters.[60] e) Normalized PL spectra for single nanocrystals with different diameters grown on the same substrate. Reproduced with permission.[60] Copyright 2016, American Chemical Society.

three orders of magnitudes. Such nanocrystal arrays arranged in a photonic crystal structure is promising for micro-LEDs with extremely stable emission, good directionality, and narrow spectral linewidth.

4. Surface-Emitting Laser Diodes

The performance of GaN-based surface-emitting laser diodes has been severely limited by the poor quality of GaN-based distributed Bragg reflectors (DBRs), which often exhibit relatively low reflectivity, large densities of dislocations, and high electrical resistivity.[67–69] Significant progress has been made in GaN-based blue vertical cavity surface emitting lasers (VCSELs) by utilizing AlInN/GaN DBRs[70] or dual-dielectric DBRs,[71] and by growing on m-plane GaN substrate.[72] Recently, surface-emitting green laser diodes have been demonstrated with the use of dual dielectric DBRs and wafer bonding to a copper plate for low thermal resistance.[73] Surface-emitting laser diodes can

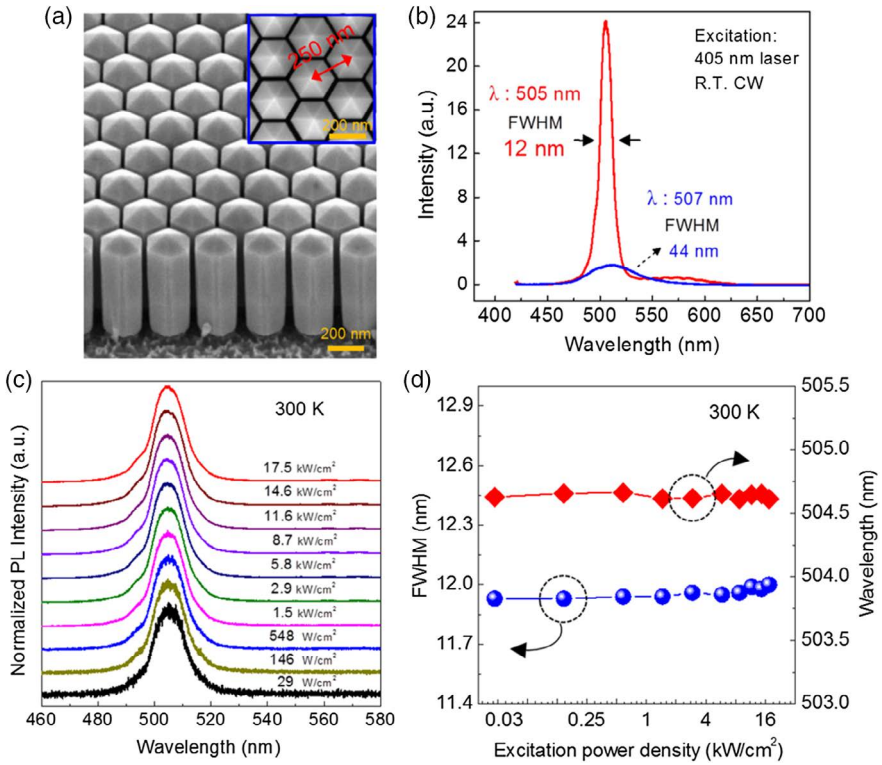

Figure 6. a) SEM image for a nanocrystal array arranged in a photonic crystal structure. b) PL spectra for nanocrystal arrays with controlled spacing (red curve) and without controlled spacing (blue curve). c) Normalized room-temperature PL spectra of a photonic crystal structure under a wide range of excitation powers from 29 W cm^{-2} to 17.5 kW cm^{-2}. d) Variations of the peak position and full-width-at-half-maximum with excitation power. Reproduced with permission.[63] Copyright 2017, Wiley-VCH Verlag GmbH & Co. KGaA.

also be readily achieved using photonic crystal structure designed to operate at Γ point.[74] **Figure 7**a shows the schematic of light scattering in the reciprocal space of a photonic crystal structure. Six Γ' points are coupled by the Bragg grating vectors K_1 and K_2, which leads to standing wave resonant in the photonic crystal structure and eliminates the need for extra mirrors for optical feedback in the X–Y plane. Furthermore, Γ point is also coupled with the six Γ' points by the Bragg grating vectors K_1 and K_2, which constitutes a path for optical output. Due to the zero in-plane wavevector k_{xy} at Γ point, the output is essentially along the vertical direction, giving the desired surface emission. The optical confinement along the vertical direction is provided by the GaN cladding layers with sufficient thicknesses below and above the active region. The active region consists of InGaN QDs and AlGaN barriers to form Al-rich shell which can suppress nonradiative surface recombination.[75–77] Our designed photonic band structure is shown in Figure 7b, which has a lattice constant of $a = 250$ nm. The normalized frequency of the Γ point of the 4th band is $\approx 0.48a/\lambda$, which corresponds to emission wavelength λ at ≈520 nm.

The fabricated surface emitting laser diode exhibits excellent current–voltage (I–V) characteristics as shown in Figure 7c. A sharp turn-on voltage of ≈3.3 V is measured at room-temperature and the leakage current under reverse bias is negligible. The emission spectra are shown in Figure 7d. Only a broad spontaneous emission spectrum with a linewidth of ≈30 nm centered at ≈524 nm was observed when the injection current is low. A sharp lasing peak with a linewidth of 0.8 nm at ≈523 nm emerged as the injection current increases. The variation of output power with injection current is shown in Figure 7e, which exhibits a threshold with a nonlinear increase around an injection current of 400 A cm^{-2}. The threshold is significantly lower than previously reported GaN VCSELs, which is related to the efficient in-plane optical feedback in the photonic crystal structure and dislocation-free InGaN nanocrystals.[70,73,78–80] The variations of the emission linewidth and peak position are shown in Figure 7f,g, respectively. The lasing peak remains stable above the threshold, which is attributed to the band edge mode at Γ point and the reduced polarization field in nanocrystals exhibiting semi-polar facets.

5. Deep UV Optoelectronics

The development of deep UV optoelectronic devices has been largely hindered by the lack of efficient p-type conduction due to the high activation energy of p-type dopant (Mg).[81–83] Recently, breakthroughs have been made by using MBE to grow high-quality Mg-doped AlN nanocrystals that can exhibit efficient p-type conduction.[23,84] This has opened up new opportunities for achieving high-efficiency deep UV LEDs and electrically pumped UV laser diodes.

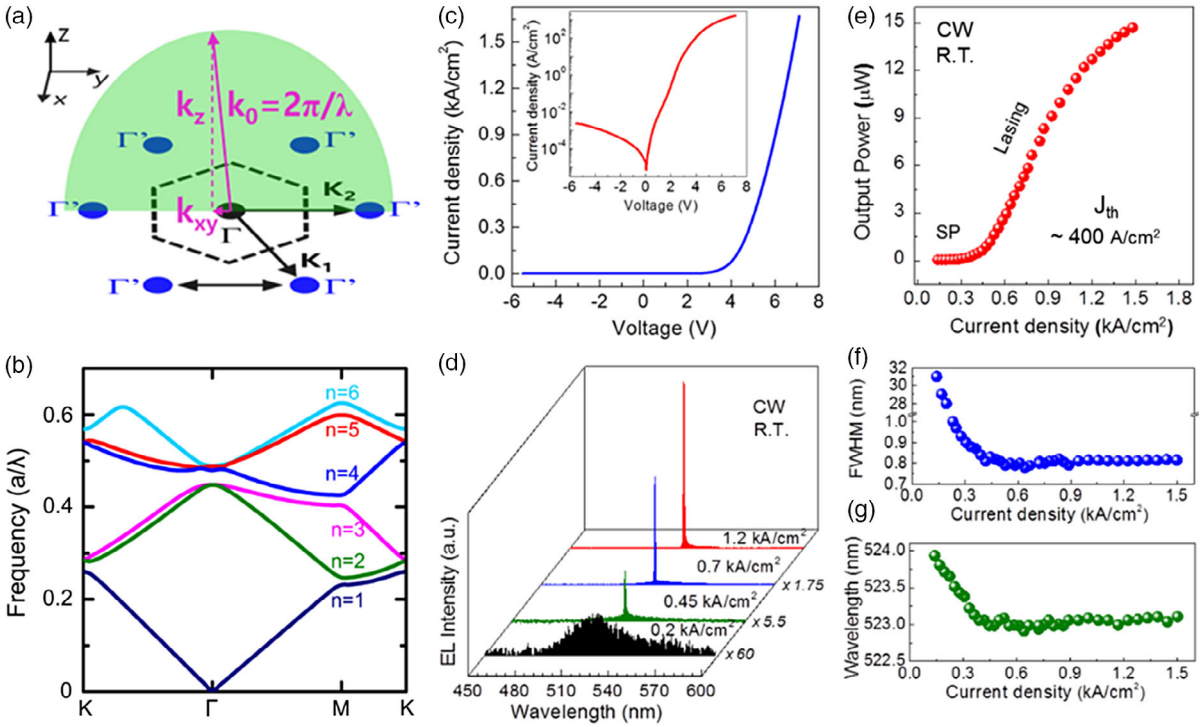

Figure 7. a) Schematic of light scattering at Γ point in a photonic crystal structure. b) Photonic bandstructure of the photonic crystal structure designed for green emission. c) *I–V* characteristics of a green laser diode. The inset displays the data on a semi-log scale. d) Emission spectra under various injection currents. e) The variation of output power with injection current. f) The variation of spectral linewidth with injection current. g) The variation of emission peak position with injection current. Rreproduced under the terms of the Creative Commons CC-BY license.[74] Copyright 2020, AAAS.

5.1. Efficient p-Type Conduction of Mg-Doped AlN Nanocrystals

The unique advantage of nanocrystal lies in the efficient incorporation of p-type Mg dopant. Theoretical studies have shown that the Ga (Al) substitutional Mg-dopant formation energy is much reduced in nanocrystals than in the bulk material, which allows for the incorporation of a high concentration of Mg dopant without extensive defect formation.[23] As the concentration of Mg dopant increases, the Mg energy levels start to interact with each other and broaden as shown in **Figure 8**a, forming an impurity band where hole conduction can occur by hopping. Moreover, some Mg-acceptor levels shift closer toward the valence band due to dispersion of their energy levels, which essentially reduces the Mg-dopant activation energy and contributes to free holes in the valance band. Figure 8b shows the PL spectra for AlN nanocrystals with Mg doping and without any intentional doping. The Mg-doped sample exhibits a pronounced peak at ≈230 nm, which is from Mg-acceptor-related transition. The energy separation between this peak and the excitonic emission of AlN is around 0.5–0.6 eV, matching the previously reported value for the activation energy of Mg-acceptor level in bulk AlN.[81,86] It is important to note that the tail of the peak at 230 nm from Mg-acceptor-related transition has an appreciable overlap with the excitonic emission peak of AlN at 210 nm, which confirms the reduced energy separation between the valence band and some Mg-acceptor levels due to the significant broadening of Mg-acceptor levels at high concentrations.

As shown in Figure 8c, the measured electrical resistivity of Mg-doped AlN nanocrystals shows a very small activation energy of 20–30 meV around room-temperature, which is explained by the dominant hole hopping conduction in the Mg impurity band.[85] When the temperature is increased, the activation energy increases to values close to commonly reported values for Mg activation energy in bulk AlN.[81,86] To further confirm the mechanism for hole current conduction, the dependence of hole concentration on temperature is studied for two Mg-doped AlN nanocrystal samples with different doping levels. The sample with relatively low Mg concentration exhibits a monotonically increasing trend for hole concentration as the temperature increases, as shown in Figure 8d.[84] The hole concentration in the sample with relatively high Mg concentration (red circles), however, exhibits a decreasing trend initially until the temperature reaches 550 K and then an increasing trend for higher temperatures. The reason for the initial decreasing trend with temperature is that the number of holes in the Mg impurity band, which dominates the overall current conduction, is reduced at elevated temperature due to ionization. When the temperature is sufficiently high (>550 K), the holes in the valence band dominate the overall current conduction, exhibiting an increasing trend with temperature as expected.

5.2. AlN and AlGaN UV LEDs and Laser Diodes

Compared with the planar LED structures, nanocrystals can enhance the light extraction efficiency for transverse magnetic

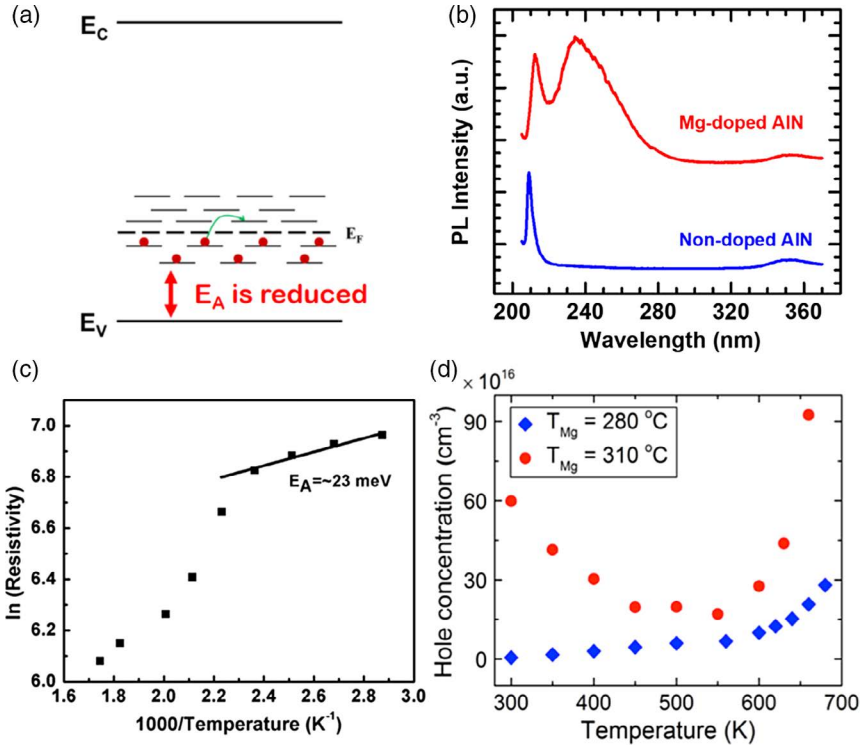

Figure 8. a) Schematic for the formation of Mg impurity band and the resultant reduced activation energy. b) PL spectra of AlN nanocrystals with and without intentional Mg-doping. c) Variation of the resistivity of heavily Mg-doped AlN nanocrystals with temperature. Reproduced with permission.[85] Copyright 2015, American Institute of Physics. d) Variation of hole concentration in heavily Mg-doped (red circles) and moderately Mg-doped (blue diamonds) AlN nanocrystals. Reproduced with permission.[84] Copyright 2017, American Institute of Physics.

polarized emission. Detailed finite-difference time-domain simulations show that the light extraction efficiency can reach more than 80% for AlGaN photonic nanocrystal LEDs.[87,88] It has also been demonstrated experimentally that nanostructures used as a highly reflective photonic crystal in backside emitting LEDs can nearly double the external quantum efficiency.[89] AlN nanocrystal LEDs have recently been demonstrated, which can exhibit a turn-on voltage ≈5.5 V at room temperature as shown in **Figure 9**a, compared with >20 V for previously reported planar c-plane AlN LEDs.[82,87] The EL spectra with a stable and pronounced peak at ≈207 nm under varying injection currents are shown in Figure 9b. By controlling the composition of AlGaN nanocrystals, AlGaN nanocrystal LEDs with emission wavelengths from ≈210 nm to ≈280 nm have also been demonstrated, as shown in Figure 9c.[23,30,76,87,90,92–95] To date, there has been only one demonstration of electrically pumped AlGaN quantum well lasers operating in the UV-B and UV-C bands.[26,91,96–100] With the use of AlGaN nanocrystals electrically pumped mid and deep UV laser diodes has been successfully demonstrated, as shown in Figure 9d.[26,96–98]

6. Artificial Photosynthesis

Artificial photosynthesis, i.e., the chemical transformation of sunlight, water and carbon dioxide into energy-rich fuels, provides an effective means for harvesting the abundant solar energy to use on demand for stationary and mobile applications.[101,102] This approach can be an ideal long-term solution to the energy-related problems and environmental remediation on a global scale.[103,104] GaN-based alloys and nanostructures exhibit near-ideal thermodynamic and kinetic attributes and advantages[105] over other known photocatalysts, including extreme chemical stability, high absorption coefficients and tunable bandgap to encompass nearly entire solar spectrum (shown in **Figure 10**) while straddling water redox potential for up to ≈50% indium incorporation.[10,106] Moreover, the nonpolar surfaces of GaN are highly reactive for spontaneous dissociation of water molecules,[107,108] and possess low energy barrier for proton diffusion.[109,110] GaN-based nanocrystals provide additional advantages, including significantly reduced defects and dislocations when grown on foreign substrates, efficient light absorption and charge carrier separation, and enhanced stability due to the N-rich surfaces that can protect against photo-corrosion and oxidation.[111–116]

6.1. Photocatalytic and Photoelectrochemical Solar Water Splitting

Our early demonstration on wafer-level water splitting confirmed, for the first time, that GaN nanowires meet the essential thermodynamic and kinetic requirements and are capable of spontaneously splitting neutral pH pure water into constituent parts, with stoichiometric H_2 and O_2 ratio of 2:1, without any

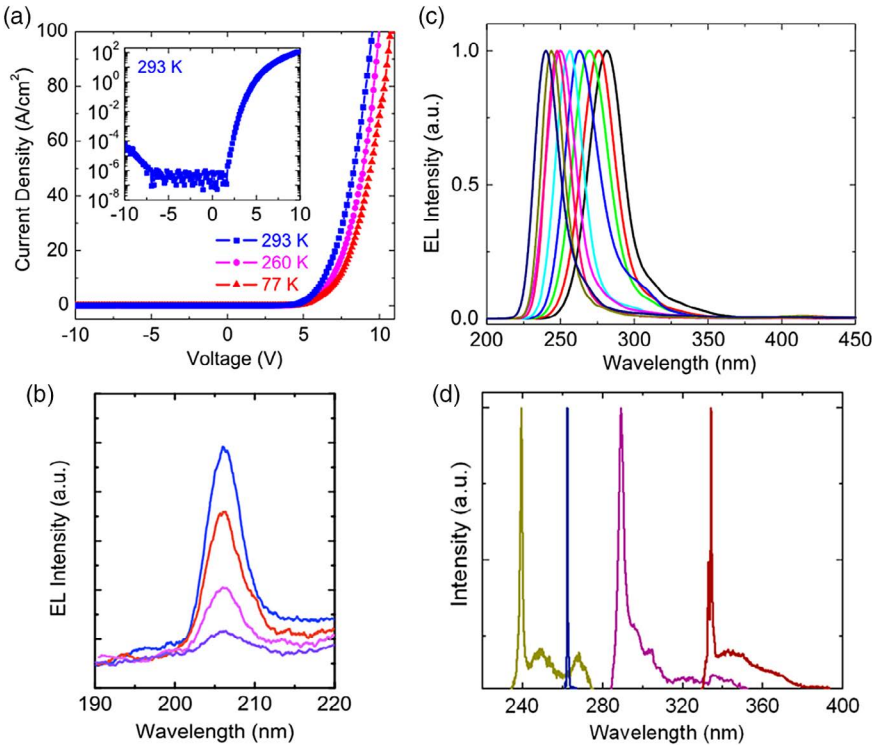

Figure 9. a) *I–V* characteristics of an AlN nanocrystal LED at different temperatures. b) EL spectra of an AlN nanocrystal LED under various injection currents. a,b) Reproduced with permission.[87] Copyright 2015, American Chemical Society. c) Normalized EL spectra of AlGaN nanocrystal LEDs with emission from ≈210 to ≈280 nm. Reproduced under the terms of the Creative Commons CC-BY license.[90] Copyright 2016, American Institute of Physics. d) Emission spectra of UV laser diodes based on AlGaN nanocrystals from UV-A band to UV-C bands. Reproduced under the terms of the Creative Commons CC-BY license.[91] Copyright 2017, The Authors, published by MDPI.

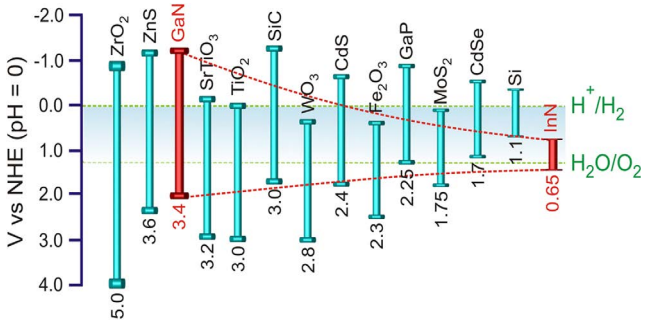

Figure 10. Bandgaps (eV) and band edge positions of commonly used photocatalysts with respect to oxidation and reduction potential of water (green dotted line). The red dotted line represents the band edge position of $In_xGa_{1-x}N$ as a function of indium incorporation (0–1 from left to right). Reproduced under the terms of the Creative Commons CC-BY license.[106] Copyright 2015, American Institute of Physics.

external bias or conductive electrolytes.[117] By optimizing the surface charge properties through controlled dopant incorporation, the H_2 evolution rate in overall solar water splitting on p-GaN nanowire device was enhanced by nearly two orders of magnitude, and the IQE can reach over ≈51%, as shown in **Figure 11**a. Dual-band p-GaN/InGaN nanowire photocatalysts can exhibit further enhanced energy conversion efficiency (ECE) of ≈7.5% and solar-to-hydrogen (STH) conversion efficiency of ≈1.8%.[106,118] To spontaneously induce charge carrier separation and to steer charge carriers toward the distinct redox sites, p-type dopant (Mg) concentrations were rationally tailored in the lateral direction of Ga(In)N photochemical diodes,[120] which induces large built-in electric field between the two parallel surfaces (≈300 meV). STH efficiency values of ≈3.3% and 5.2% had been measured on such Ga(In)N photochemical diodes and quadruple-band devices, respectively, which are significantly higher than previously reported efficiency values for neutral pH one-step overall water splitting.[121–126] Recent studies demonstrated that simultaneous loading of water oxidation and proton reduction cocatalysts (Co_3O_4 and Rh/Cr_2O_3) on p-GaN/InGaN nanowires can efficiently drive the unassisted overall water splitting for more than ≈580 h under concentrated sunlight (equivalent to 27 Suns), as shown in Figure 11b.[119] Such device longevity is unique for any inorganic semiconductor photocatalysts or photoelectrodes without any protection layer for unbiased overall photocatalytic pure water splitting with STH > 1%. Systematic investigation, both theoretical and experimental, on the atomic-scale origin of such long-term stability and high efficiency revealed that the Ga(In)N nanowires grown by MBE can spontaneously form atomically thin N-terminated layers, on both their polar top surfaces and lateral nonpolar sidewalls as shown in **Figure 12**.[116] Such a unique surface configuration passivates the nanowires against attack by air/aqueous electrolytes.[127]

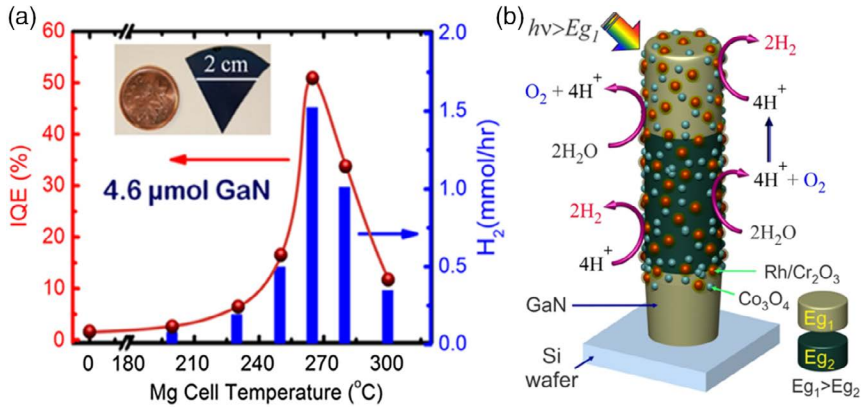

Figure 11. a) IQE and corresponding hydrogen evolution from GaN samples, doped at different Mg effusion cell temperature. The inset shows the relative size of sample substrate. The area exposed to irradiation for redox reaction was ≈2.8 cm^2. Reproduced with permission.[118] Copyright 2015, Nature Research. b) Schematic illustration of unassisted overall pure water splitting on a dual-cocatalyst loaded double-band nanowire heterostructure (herein, $E_{g1} \approx 3.4$ eV and $E_{g2} \approx 2.46$ eV). Water oxidation (O_2 evolution) is promoted on Co_3O_4, whereas Rh/Cr_2O_3 promotes the proton reduction reaction (H_2 evolution). Reproduced with permission.[119] Copyright 2018, American Chemical Society.

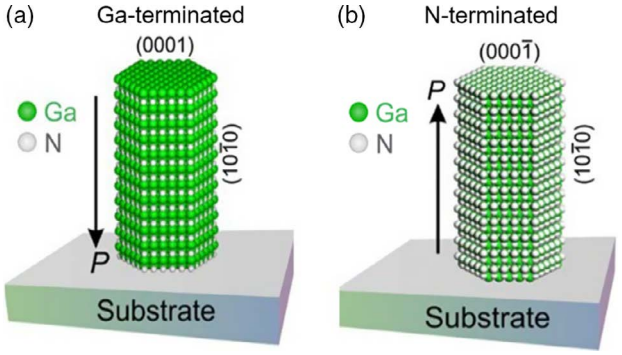

Figure 12. Model for single crystal wurtzite GaN nanowire with a polar a) Ga-terminated (0001) top surface and (10$\bar{1}$0) surface, and b) N-terminated (000$\bar{1}$) top surface and N-terminated (10$\bar{1}$0) and C_{6v}-symmetric side faces, obtained by removal of the surface Ga atoms which causes N—Ga bonds to be broken and to the re-orientation of the N bond orbitals. *P* represents the direction of spontaneous polarization of the wurtzite crystal. Reproduced with permission.[116] Copyright 2016, Wiley-VCH Verlag GmbH & Co. KGaA.

Recently, Vanka et al. demonstrated GaN nanowire protected Si photocathodes exhibit excellent performance, including a saturated photocurrent density of ≈38 mA cm^{-2}, a large applied bias photon-to-current efficiency of 10.5%.[128,129] Chronoamperometry analysis for the photocathode shows a stable photocurrent density of ≈38 mA cm^{-2} for ≈3000 h without degradation, which is the best reported stability for a semiconductor photocathode at a photocurrent density of 35 mA cm^{-2}, or higher under one-sun illumination. Wang et al. reported a GaInP/GaAs/Ge triple-junction photocathode protected by multifunctional GaN nanostructures can enable both efficient and relatively stable solar water splitting.[130] A 12.6% STH efficiency is measured without any external bias and relatively stable solar water splitting for 80 h in three-electrode configuration and 57 h in two-electrode measurement at zero bias.

Recent investigations further revealed that the industry-ready GaN-based artificial photosynthetic system can be realized with enhanced efficiency and stability by using highly crystalline, low-bandgap (≈1.5 eV) nanostructures for extended visible light absorption (e.g., In-rich InGaN, dilute-antimonide GaInSbN, etc.)[131–133] that can reduce the gas evolution overpotentials for both half-reactions via bandgap and band-edge tuning, by controllably introducing donor/acceptor states into the bandgap[134] and using dye-sensitization approach for efficient and stable solar water splitting under deep-visible and near-infrared irradiation.[135]

6.2. Chemical Transformation of CO_2 to Fuels

The photo(electro)chemical reduction of CO_2 into value-added chemicals and fuels (e.g., CO, HCOOH, CH_3OH, and CH_4) using solar energy has received considerable attention. Compared with most metal oxides, the conduction band minimum of GaN is more negative and hence sufficient to meet the thermodynamic requirements for CO_2 reduction. Kinetically, it is important to couple with suitable cocatalyst to enhance the charge separation and activate the stable CO_2 molecule into desired products with high selectivity. By using Rh/Cr_2O_3 or Pt as cocatalysts, GaN nanowire arrays has been demonstrated for photochemical CO_2 reduction with H_2O into CH_4 with a production rate of 3.5 and 14.8 μmol g_{cat}^{-1} h^{-1}, respectively.[136] With the use of Pt-modified p-InGaN/GaN nanowire arrays, visible-light-driven CO_2 conversion with H_2 into CH_3OH, CO and CH_4 has been achieved with an evolution rate of ≈0.5, 0.1, and 0.25 mmol g_{cat}^{-1} h^{-1}, respectively.[137] In addition to the photochemical system, GaN nanowire arrays integrated with Si substrate has emerged as a powerful platform for photoelectrochemical CO_2 reduction, taking advantages of strong light absorption capability of Si (bandgap of 1.1 eV) and effective electron extraction as well as high surface area of GaN nanowires. Such a GaN/Si platform has emerged as a fundamental framework to understand the effect of various cocatalysts on

the selectivity of photoelectrochemical CO_2 reduction. With the incorporation of Cu as the cocatalyst, the device exhibited a Faradaic efficiency of 19% for CH_4 generation.[138] When using a synergetic cocatalytic effect between Cu and ZnO, the device demonstrated a tunable syngas generation with CO/H_2 ratio ranging from 2:1 to 1:4.[139] Furthermore, by using Pt/TiO_2 as a model cocatalyst for constructing metal/oxide interface, the resulting photoelectrode yielded a solar-to-syngas efficiency of 0.87% with an adjustable CO/H_2 ratio between 4:1 and 1:6.[140] Very recently, using Sn and binary Cu–Ir as the cocatalysts, high Faradaic efficiency values of 77% for HCOOH formation and 51% for methane production have been reported, respectively.[141,142] Nanoscale III-nitrides have also been used for the synthesis of "green" ammonia[143] and ethanol[144] through light-driven chemical reactions.

7. Conclusion

III-nitride nanocrystals have emerged as a unique platform and provide distinct opportunities to address many critical challenges we face today, including the realization of low defect density templates with arbitrary In (or Al) compositions, efficient multi-color micro LEDs, high-performance deep UV optoelectronic devices, and high-efficiency solar energy and artificial photosynthesis devices and systems. In addition, they have been studied for applications in low-power logic and memory devices, as well as the emerging quantum devices through heterogeneous integration and quantum engineering.[145–166]

Acknowledgements

This work was supported by US Army Research Office (W911NF-17-1-0109) and National Science Foundation (ECCS-1709207).

Conflict of Interest

Part of the IP related to some of the work presented in this article was licensed to NS Nanotech, Inc., which was co-founded by Z.M.

Keywords

III-nitrides, artificial photosynthesis, deep ultraviolet photonics, nanocrystals, photonic crystals

Received: October 25, 2019
Revised: January 22, 2020
Published online:

[1] S. Pimputkar, J. S. Speck, S. P. DenBaars, S. Nakamura, *Nat. Photonics* **2009**, *3*, 180.
[2] S. Moon, G. Koo, G. Moon, *IEEE Trans. Power Electron.* **2013**, *28*, 4051.
[3] A. Sanchot, M. Consonni, S. Le Calvez, I. C. Robin, F. Templier, *MRS Proc.* **2015**, *1788*, 19.
[4] K. Boutros, R. Chu, B. Hughes, presented at *Proceedings of the IEEE 2013 Custom Integrated Circuits Conference*, San Jose, CA, September **2013**.
[5] K. S. Boutros, R. Chu, B. Hughes, presented at *2012 IEEE Energytech*, Cleveland, OH, May **2012**.
[6] T. Mukai, M. Yamada, S. Nakamura, *Jpn. J. Appl. Phys.* **1999**, *38*, 3976.
[7] H. Hirayama, S. Fujikawa, N. Noguchi, J. Norimatsu, T. Takano, K. Tsubaki, N. Kamata, *Phys. Status Solidi A* **2009**, *206*, 1176.
[8] H. Hirayama, T. Yatabe, N. Noguchi, T. Ohashi, N. Kamata, *Phys. Status Solidi C* **2008**, *5*, 2969.
[9] T. Kolbe, F. Mehnke, M. Guttmann, C. Kuhn, J. Rass, T. Wernicke, M. Kneissl, *Appl. Phys. Lett.* **2013**, *103*, 031109.
[10] P. G. Moses, C. G. V. d. Walle, *Appl. Phys. Lett.* **2010**, *96*, 021908.
[11] M. G. Kibria, Z. Mi, *J. Mater. Chem. A* **2016**, *4*, 2801.
[12] M. César, Y. Ke, W. Ji, H. Guo, Z. Mi, *Appl. Phys. Lett.* **2011**, *98*, 202107.
[13] R. Yoshizawa, H. Miyake, K. Hiramatsu, *Jpn. J. Appl. Phys.* **2017**, *57*, 01AD05.
[14] H. Miyake, C.-H. Lin, K. Tokoro, K. Hiramatsu, *J. Cryst. Growth* **2016**, *456*, 155.
[15] H. Miyake, G. Nishio, S. Suzuki, K. Hiramatsu, H. Fukuyama, J. Kaur, N. Kuwano, *Appl. Phys. Express* **2016**, *9*, 025501.
[16] S. Xiao, N. Jiang, K. Shojiki, K. Uesugi, H. Miyake, *Jpn. J. Appl. Phys.* **2019**, *58*, SC1003.
[17] L. Zhang, F. Xu, J. Wang, C. He, W. Guo, M. Wang, B. Sheng, L. Lu, Z. Qin, X. Wang, B. Shen, *Sci. Rep.* **2016**, *6*, 35934.
[18] P. Dong, J. Yan, J. Wang, Y. Zhang, C. Geng, T. Wei, P. Cong, Y. Zhang, J. Zeng, Y. Tian, L. Sun, Q. Yan, J. Li, S. Fan, Z. Qin, *Appl. Phys. Lett.* **2013**, *102*, 241113.
[19] M. Conroy, V. Z. Zubialevich, H. Li, N. Petkov, J. D. Holmes, P. J. Parbrook, *J. Mater. Chem. C* **2015**, *3*, 431.
[20] S. P. Young, B. R. Hwang, J. C. Lee, I. Hyunsik, H. Y. Cho, T. W. Kang, J. H. Na, C. M. Park, *Nanotechnology* **2006**, *17*, 4640.
[21] J. Ristić, M. A. Sánchez-García, E. Calleja, J. Sanchez-Páramo, J. M. Calleja, U. Jahn, K. H. Ploog, *Phys. Status Solidi A* **2002**, *192*, 60.
[22] K. A. Bertness, A. Roshko, N. A. Sanford, J. M. Barker, A. V. Davydov, *J. Cryst. Growth* **2006**, *287*, 522.
[23] S. Zhao, A. T. Connie, M. H. T. Dastjerdi, X. H. Kong, Q. Wang, M. Djavid, S. Sadaf, X. D. Liu, I. Shih, H. Guo, Z. Mi, *Sci. Rep.* **2015**, *5*, 8332.
[24] F. K. Thomas, D. C. Santino, A. T. M. Sarwar, J. P. Patrick, F. K. Robert, C. M. Roberto, *Nanotechnology* **2014**, *25*, 455201.
[25] S. D. Carnevale, T. F. Kent, P. J. Phillips, A. T. M. G. Sarwar, C. Selcu, R. F. Klie, R. C. Myers, *Nano Lett.* **2013**, *13*, 3029.
[26] S. Zhao, S. Y. Woo, M. Bugnet, X. Liu, J. Kang, G. A. Botton, Z. Mi, *Nano Lett.* **2015**, *15*, 7801.
[27] A. Pierret, C. Bougerol, S. Murcia-Mascaros, A. Cros, H. Renevier, B. Gayral, B. Daudin, *Nanotechnology* **2013**, *24*, 115704.
[28] A. Pierret, C. Bougerol, M. D. Hertog, B. Gayral, M. Kociak, H. Renevier, B. Daudin, *Phys. Status Solidi RRL* **2013**, *7*, 868.
[29] Y. Wu, Y. Wang, K. Sun, Z. Mi, *J. Cryst. Growth* **2019**, *507*, 65.
[30] B. Janjua, H. Sun, C. Zhao, D. H. Anjum, D. Priante, A. A. Alhamoud, F. Wu, X. Li, A. M. Albadri, A. Y. Alyamani, M. M. El-Desouki, T. K. Ng, B. S. Ooi, *Opt. Express* **2017**, *25*, 1381.
[31] M. Yoshizawa, A. Kikuchi, M. Mori, N. Fujita, K. Kishino, *Jpn. J. Appl. Phys.* **1997**, *36*, L459.
[32] M. Yoshizawa, A. Kikuchi, N. Fujita, K. Kushi, H. Sasamoto, K. Kishino, *J. Cryst. Growth* **1998**, *189–190*, 138.
[33] E. Calleja, M. A. Sánchez-García, F. J. Sánchez, F. Calle, F. B. Naranjo, E. Muñoz, U. Jahn, K. Ploog, *Phys. Rev. B* **2000**, *62*, 16826.
[34] T. Stoica, R. Calarco, *IEEE J. Sel. Top. Quantum Electron.* **2011**, *17*, 859.
[35] L. Geelhaar, C. Chèze, B. Jenichen, O. Brandt, C. Pfüller, S. Münch, R. Rothemund, S. Reitzenstein, A. Forchel, T. Kehagias, P. Komninou, G. P. Dimitrakopulos, T. Karakostas, L. Lari, P. R. Chalker, M. H. Gass, H. Riechert, *IEEE J. Sel. Top. Quantum Electron.* **2011**, *17*, 878.

[36] K. A. Bertness, N. A. Sanford, A. V. Davydov, *IEEE J. Sel. Top. Quantum Electron.* **2011**, *17*, 847.
[37] R. Mata, K. Hestroffer, J. Budagosky, A. Cros, C. Bougerol, H. Renevier, B. Daudin, *J. Cryst. Growth* **2011**, *334*, 177.
[38] S. D. Hersee, M. Fairchild, A. K. Rishinaramangalam, M. S. Ferdous, L. Zhang, P. M. Varangis, B. S. Swartzentruber, A. A. Talin, *Electron. Lett.* **2009**, *45*, 75.
[39] M. Knelangen, V. Consonni, A. Trampert, H. Riechert, *Nanotechnology* **2010**, *21*, 245705.
[40] T. Schumann, T. Gotschke, F. Limbach, T. Stoica, R. Calarco, *Nanotechnology* **2011**, *22*, 095603.
[41] S. D. Hersee, X. Sun, X. Wang, *Nano Lett.* **2006**, *6*, 1808.
[42] C. Liu, P. A. Shields, Q. Chen, D. W. E. Allsopp, W. N. Wang, C. R. Bowen, T.-L. Phan, D. Cherns, *Phys. Status Solidi C* **2010**, *7*, 32.
[43] K. Choi, M. Arita, Y. Arakawa, *J. Cryst. Growth* **2012**, *357*, 58.
[44] J. E. Kruse, L. Lymperakis, S. Eftychis, A. Adikimenakis, G. Doundoulakis, K. Tsagaraki, M. Androulidaki, A. Olziersky, P. Dimitrakis, V. Ioannou-Sougleridis, P. Normand, T. Koukoula, T. Kehagias, P. Komninou, G. Konstantinidis, A. Georgakilas, *J. Appl. Phys.* **2016**, *119*, 224305.
[45] Q. Li, Y. Lin, J. R. Creighton, J. J. Figiel, G. T. Wang, *Adv. Mater.* **2009**, *21*, 2416.
[46] P. Dogan, O. Brandt, C. Pfüller, J. Lähnemann, U. Jahn, C. Roder, A. Trampert, L. Geelhaar, H. Riechert, *Cryst. Growth Des.* **2011**, *11*, 4257.
[47] S. Fan, S. Zhao, X. Liu, Z. Mi, *J. Vac. Sci. Technol. B* **2014**, *32*, 02C114.
[48] B. H. Le, S. Zhao, X. Liu, S. Y. Woo, G. A. Botton, Z. Mi, *Adv. Mater.* **2016**, *28*, 8446.
[49] B. Jenichen, O. Brandt, C. Pfüller, P. Dogan, M. Knelangen, A. Trampert, *Nanotechnology* **2011**, *22*, 295714.
[50] V. M. Kaganer, B. Jenichen, O. Brandt, S. Fernández-Garrido, P. Dogan, L. Geelhaar, H. Riechert, *Phys. Rev. B* **2012**, *86*, 115325.
[51] S. Fernández-Garrido, V. M. Kaganer, C. Hauswald, B. Jenichen, M. Ramsteiner, V. Consonni, L. Geelhaar, O. Brandt, *Nanotechnology* **2014**, *25*, 455702.
[52] J. F. Kaeding, H. Asamizu, H. Sato, M. Iza, T. E. Mates, S. P. DenBaars, J. S. Speck, S. Nakamura, *Appl. Phys. Lett.* **2006**, *89*, 202104.
[53] L. Lahourcade, J. Pernot, A. Wirthmüller, M. P. Chauvat, P. Ruterana, A. Laufer, M. Eickhoff, E. Monroy, *Appl. Phys. Lett.* **2009**, *95*, 171908.
[54] F. Glas, *Phys. Rev. B* **2006**, *74*, 121302.
[55] A. K. Rishinaramangalam, M. Nami, M. N. Fairchild, D. M. Shima, G. Balakrishnan, S. R. J. Brueck, D. F. Feezell, *Appl. Phys. Express* **2016**, *9*, 032101.
[56] M. L. Nakarmi, K. H. Kim, M. Khizar, Z. Y. Fan, J. Y. Lin, H. X. Jiang, *Appl. Phys. Lett.* **2005**, *86*, 092108.
[57] M. L. Nakarmi, K. H. Kim, J. Li, J. Y. Lin, H. X. Jiang, *Appl. Phys. Lett.* **2003**, *82*, 3041.
[58] T. Kinoshita, T. Obata, H. Yanagi, S.-I. Inoue, *Appl. Phys. Lett.* **2013**, *102*, 012105.
[59] H. M. Ng, D. Doppalapudi, D. Korakakis, R. Singh, T. D. Moustakas, *J. Cryst. Growth* **1998**, *189–190*, 349.
[60] Y.-H. Ra, R. Wang, S. Y. Woo, M. Djavid, S. M. Sadaf, J. Lee, G. A. Botton, Z. Mi, *Nano Lett.* **2016**, *16*, 4608.
[61] H. Sekiguchi, K. Kishino, A. Kikuchi, *Appl. Phys. Lett.* **2010**, *96*, 231104.
[62] N. Sakakibara, K. Narita, T. Oto, K. Kishino, presented at *2017 22nd Microoptics Conference (MOC)*, Tokyo, Japan, November **2017**.
[63] Y.-H. Ra, R. T. Rashid, X. Liu, J. Lee, Z. Mi, *Adv. Funct. Mater.* **2017**, *27*, 1702364.
[64] M. Boroditsky, R. Vrijen, T. F. Krauss, R. Coccioli, R. Bhat, E. Yablonovitch, *J. Lightw. Technol.* **1999**, *17*, 2096.
[65] C.-F. Huang, C.-Y. Chen, C.-F. Lu, C. C. Yang, *Appl. Phys. Lett.* **2007**, *91*, 051121.
[66] M. Strassburg, A. Hoffmann, J. Holst, J. Christen, T. Riemann, F. Bertram, P. Fischer, *Phys. Status Solidi C* **2003**, *0*, 1835.
[67] R. F. Kopf, E. F. Schubert, S. W. Downey, A. B. Emerson, *Appl. Phys. Lett.* **1992**, *61*, 1820.
[68] J.-F. Carlin, C. Zellweger, J. Dorsaz, S. Nicolay, G. Christmann, E. Feltin, R. Butté, N. Grandjean, *Phys. Status Solidi B* **2005**, *242*, 2326.
[69] S.-M. Lee, S.-H. Gong, J.-H. Kang, M. Ebaid, S.-W. Ryu, Y.-H. Cho, *Opt. Express* **2015**, *23*, 11023.
[70] G. Cosendey, A. Castiglia, G. Rossbach, J.-F. Carlin, N. Grandjean, *Appl. Phys. Lett.* **2012**, *101*, 151113.
[71] T. Lu, J. Chen, S. Chen, H. Kuo, C. Kuo, C. Lee, S. Wang, *IEEE J. Sel. Top. Quantum Electron.* **2009**, *15*, 850.
[72] C. Holder, J. S. Speck, S. P. DenBaars, S. Nakamura, D. Feezell, *Appl. Phys. Express* **2012**, *5*, 092104.
[73] Y. Mei, G.-E. Weng, B.-P. Zhang, J.-P. Liu, W. Hofmann, L.-Y. Ying, J.-Y. Zhang, Z.-C. Li, H. Yang, H.-C. Kuo, *Light Sci. Appl.* **2017**, *6*, e16199.
[74] Y.-H. Ra, R. T. Rashid, X. Liu, S. M. Sadaf, K. Mashooq, Z. Mi, *Sci. Adv.* **2020**, *6*, eaav7523.
[75] X. Liu, B. H. Le, S. Y. Woo, S. Zhao, A. Pofelski, G. A. Botton, Z. Mi, *Opt. Express* **2017**, *25*, 30494.
[76] Q. Wang, H. P. T. Nguyen, K. Cui, Z. Mi, *Appl. Phys. Lett.* **2012**, *101*, 043115.
[77] R. Wang, X. Liu, I. Shih, Z. Mi, *Appl. Phys. Lett.* **2015**, *106*, 261104.
[78] H. Matsubara, S. Yoshimoto, H. Saito, Y. Jianglin, Y. Tanaka, S. Noda, *Science* **2008**, *319*, 445.
[79] P. S. Yeh, C.-C. Chang, Y.-T. Chen, D.-W. Lin, J.-S. Liou, C. C. Wu, J. H. He, H.-C. Kuo, *Appl. Phys. Lett.* **2016**, *109*, 241103.
[80] T. Hamaguchi, N. Fuutagawa, S. Izumi, M. Murayama, H. Narui, *Phys. Status Solidi A* **2016**, *213*, 1170.
[81] M. L. Nakarmi, N. Nepal, C. Ugolini, T. M. Altahtamouni, J. Y. Lin, H. X. Jiang, *Appl. Phys. Lett.* **2006**, *89*, 152120.
[82] Y. Taniyasu, M. Kasu, T. Makimoto, *Nature* **2006**, *441*, 325.
[83] U. Kaufmann, P. Schlotter, H. Obloh, K. Köhler, M. Maier, *Phys. Rev. B* **2000**, *62*, 10867.
[84] N. H. Tran, B. H. Le, S. Zhao, Z. Mi, *Appl. Phys. Lett.* **2017**, *110*, 032102.
[85] A. T. Connie, S. Zhao, S. M. Sadaf, I. Shih, Z. Mi, X. Du, J. Lin, H. Jiang, *Appl. Phys. Lett.* **2015**, *106*, 213105.
[86] K. B. Nam, M. L. Nakarmi, J. Li, J. Y. Lin, H. X. Jiang, *Appl. Phys. Lett.* **2003**, *83*, 878.
[87] S. Zhao, M. Djavid, Z. Mi, *Nano Lett.* **2015**, *15*, 7006.
[88] X. Liu, K. Mashooq, T. Szkopek, Z. Mi, *IEEE Photon. J.* **2018**, *10*, 1.
[89] Y. Kashima, N. Maeda, E. Matsuura, M. Jo, T. Iwai, T. Morita, M. Kokubo, T. Tashiro, R. Kamimura, Y. Osada, H. Takagi, H. Hirayama, *Appl. Phys. Express* **2017**, *11*, 012101.
[90] S. Zhao, S. Y. Woo, S. M. Sadaf, Y. Wu, A. Pofelski, D. A. Laleyan, R. T. Rashid, Y. Wang, G. A. Botton, Z. Mi, *APL Mater.* **2016**, *4*, 086115.
[91] S. Zhao, Z. Mi, *Crystals* **2017**, *7*, 268.
[92] T. F. Kent, S. D. Carnevale, A. T. M. Sarwar, P. J. Phillips, R. F. Klie, R. C. Myers, *Nanotechnology* **2014**, *25*, 455201.
[93] S. D. Carnevale, T. F. Kent, P. J. Phillips, M. J. Mills, S. Rajan, R. C. Myers, *Nano Lett.* **2012**, *12*, 915.
[94] S. M. Sadaf, S. Zhao, Y. Wu, Y. H. Ra, X. Liu, S. Vanka, Z. Mi, *Nano Lett.* **2017**, *17*, 1212.
[95] S. Zhao, S. M. Sadaf, S. Vanka, Y. Wang, R. Rashid, Z. Mi, *Appl. Phys. Lett.* **2016**, *109*, 201106.
[96] K. H. Li, X. Liu, Q. Wang, S. Zhao, Z. Mi, *Nat. Nanotech.* **2015**, *10*, 140.
[97] S. Zhao, X. Liu, S. Y. Woo, J. Kang, G. A. Botton, Z. Mi, *Appl. Phys. Lett.* **2015**, *107*, 043101.

[98] S. Zhao, X. Liu, Y. Wu, Z. Mi, *Appl. Phys. Lett.* **2016**, *109*, 191106.
[99] C.-H. Liao, H. Sun, X. Li, in Nanoscale Semiconductor Lasers (Eds: C. Tong, C. Jagadish), Elsevier, Amsterdam **2019**, p. 139.
[100] Z. Zhang, M. Kushimoto, T. Sakai, N. Sugiyama, L. J. Schowalter, C. Sasaoka, H. Amano, *Appl. Phys. Express* **2019**, *12*, 124003.
[101] J. Su, L. Vayssieres, *ACS Energy Lett.* **2016**, *1*, 121.
[102] N. S. Lewis, D. G. Nocera, *Proc. Natl. Acad. Sci.* **2006**, *103*, 15729.
[103] J. A. Turner, M. C. Williams, K. Rajeshwar, *Electrochem. Soc. Interface Fall* **2004**, *13*, 24.
[104] J. R. Bolton, *Sol. Energy* **1996**, *57*, 37.
[105] A. Kudo, Y. Miseki, *Chem. Soc. Rev.* **2009**, *38*, 253.
[106] F. A. Chowdhury, Z. Mi, M. G. Kibria, M. L. Trudeau, *APL Mater.* **2015**, *3*, 104408.
[107] X. Shen, Y. A. Small, J. Wang, P. B. Allen, M. V. Fernandez-Serra, M. S. Hybertsen, J. T. Muckerman, *J. Phys. Chem. C* **2010**, *114*, 13695.
[108] P.-T. Chen, C.-L. Sun, M. Hayashi, *J. Phys. Chem. C* **2010**, *114*, 18228.
[109] J. Yang, D. Wang, H. Han, C. Li, *Acc. Chem. Res.* **2013**, *46*, 1900.
[110] X. Shen, P. B. Allen, M. S. Hybertsen, J. T. Muckerman, *J. Phys. Chem. C* **2009**, *113*, 3365.
[111] C. G. Van de Walle, D. Segev, *J. Appl. Phys.* **2007**, *101*, 081704.
[112] Z. Z. Bandić, P. M. Bridger, E. C. Piquette, T. C. McGill, *Appl. Phys. Lett.* **1998**, *72*, 3166.
[113] S. C. Jain, M. Willander, J. Narayan, R. V. Overstraeten, *J. Appl. Phys.* **2000**, *87*, 965.
[114] B. Monemar, G. Pozina, *Prog. Quant. Electron.* **2000**, *24*, 239.
[115] F. K. Yam, Z. Hassan, *Superlattices Microstruct.* **2008**, *43*, 1.
[116] M. G. Kibria, R. Qiao, W. Yang, I. Boukahil, X. Kong, F. A. Chowdhury, M. L. Trudeau, W. Ji, H. Guo, F. Himpsel, *Adv. Mater.* **2016**, *28*, 8388.
[117] D. Wang, A. Pierre, M. G. Kibria, K. Cui, X. Han, K. H. Bevan, H. Guo, S. Paradis, A.-R. Hakima, Z. Mi, *Nano Lett.* **2011**, *11*, 2353.
[118] M. G. Kibria, F. A. Chowdhury, S. Zhao, B. AlOtaibi, M. L. Trudeau, H. Guo, Z. Mi, *Nat. Commun.* **2015**, *6*, 6797.
[119] X. Guan, F. A. Chowdhury, Y. Wang, N. Pant, S. Vanka, M. L. Trudeau, L. Guo, L. Vayssieres, Z. Mi, *ACS Energy Lett.* **2018**, *3*, 2230.
[120] F. A. Chowdhury, M. L. Trudeau, H. Guo, Z. Mi, *Nat. Commun.* **2018**, *9*, 1707.
[121] S. Y. Reece, J. A. Hamel, K. Sung, T. D. Jarvi, A. J. Esswein, J. J. H. Pijpers, D. G. Nocera, *Science* **2011**, *334*, 645.
[122] J. H. Kim, Y. Jo, J. H. Kim, J. W. Jang, H. J. Kang, Y. H. Lee, D. S. Kim, Y. Jun, J. S. Lee, *ACS Nano* **2015**, *9*, 11820.
[123] J. Liu, Y. Liu, N. Liu, Y. Han, X. Zhang, H. Huang, Y. Lifshitz, S.-T. Lee, J. Zhong, Z. Kang, *Science* **2015**, *347*, 970.
[124] Q. Wang, T. Hisatomi, Y. Suzuki, Z. Pan, J. Seo, M. Katayama, T. Minegishi, H. Nishiyama, T. Takata, K. Seki, A. Kudo, T. Yamada, K. Domen, *J. Am. Chem. Soc.* **2017**, *139*, 1675.
[125] Y. Wang, Y. Wu, K. Sun, Z. Mi, *Mater. Horizons* **2019**, *6*, 1454.
[126] F. A. Chowdhury, *MRS Adv.* **2019**, *4*, 2771.
[127] Y. L. Chang, F. Li, A. Fatehi, Z. T. Mi, *Nanotechnology* **2009**, *20*, 6.
[128] S. Vanka, E. Arca, S. Cheng, K. Sun, G. A. Botton, G. Teeter, Z. Mi, *Nano Lett.* **2018**, *18*, 6530.
[129] S. Vanka, K. Sun, G. Zeng, T. A. Pham, F. M. Toma, T. Ogitsu, Z. Mi, *J. Mater. Chem. A* **2019**, *7*, 27612.
[130] Y. Wang, J. Schwartz, J. Gim, R. Hovden, Z. Mi, *ACS Energy Lett.* **2019**, *4*, 1541.
[131] F. A. Chowdhury, S. M. Sadaf, Q. Shi, Y.-C. Chen, H. Guo, Z. Mi, *Appl. Phys. Lett.* **2017**, *111*, 061101.
[132] Q. Shi, Y.-C. Chen, F. A. Chowdhury, Z. Mi, V. Michaud-Rioux, H. Guo, *Phys. Rev. Mater.* **2017**, *1*, 034602.
[133] F. A. Chowdhury, Z. Mi, *J. Appl. Phys.* **2019**, *126*, 085704.
[134] M. G. Kibria, F. A. Chowdhury, S. Zhao, M. L. Trudeau, H. Guo, Z. Mi, *Appl. Phys. Lett.* **2015**, *106*, 113105.
[135] M. G. Kibria, F. A. Chowdhury, M. L. Trudeau, H. Guo, Z. Mi, *Nanotechnology* **2015**, *26*, 285401.
[136] B. AlOtaibi, S. Z. Fan, D. F. Wang, J. H. Ye, Z. T. Mi, *ACS Catal.* **2015**, *5*, 5342.
[137] B. AlOtaibi, X. Kong, S. Vanka, S. Y.-M. Woo, A. Pofelski, F. Oudjedi, S. Fan, M. G. Kibria, G. A. Botton, W. Ji, *ACS Energy Lett.* **2016**, *1*, 246.
[138] Y. Wang, S. Fan, B. AlOtaibi, Y. Wang, L. Li, Z. Mi, *Chemistry* **2016**, *22*, 8809.
[139] S. Chu, S. Z. Fan, Y. J. Wang, D. Rossouw, Y. C. Wang, G. A. Botton, Z. T. Mi, *Angew Chem., Int. Ed.* **2016**, *55*, 14260.
[140] S. Chu, P. Ou, P. Ghamari, S. Vanka, B. Zhou, I. Shih, J. Song, Z. Mi, *J. Am. Chem. Soc.* **2018**, *140*, 7869.
[141] B. Zhou, X. Kong, S. Vanka, S. Cheng, N. Pant, S. Chu, P. Ghamari, Y. Wang, G. Botton, H. Cuo, Z. Mi, *Energy Environ. Sci.* **2019**, *12*, 2842.
[142] B. Zhou, P. Ou, N. Pant, S. Cheng, S. Vanka, S. Chu, R. T. Rashid, G. Botton, J. Song, Z. Mi, *Proc. Natl. Acad. Sci.* **2020**, *117*, 1330.
[143] L. Li, Y. Wang, S. Vanka, X. Mu, Z. Mi, C.-J. Li, *Angew Chem., Int. Ed.* **2017**, *56*, 8701.
[144] M. Liu, Y. Wang, X. Kong, R. T. Rashid, S. Chu, C.-C. Li, Z. Hearne, H. Guo, Z. Mi, C.-J. Li, *Chem* **2019**, *5*, 858.
[145] M. F. Fatahilah, F. Yu, K. Strempel, F. Römer, D. Maradan, M. Meneghini, A. Bakin, F. Hohls, H. W. Schumacher, B. Witzigmann, A. Waag, H. S. Wasisto, *Sci. Rep.* **2019**, *9*, 10301.
[146] Y. Huang, X. Duan, Y. Cui, C. M. Lieber, *Nano Lett.* **2002**, *2*, 101.
[147] A. Motayed, M. He, A. V. Davydov, J. Melngailis, S. N. Mohammad, *J. Appl. Phys.* **2006**, *100*, 114310.
[148] H.-Y. Cha, H. Wu, M. Chandrashekhar, Y. C. Choi, S. Chae, G. Koley, M. G. Spencer, *Nanotechnology* **2006**, *17*, 1264.
[149] P. T. Blanchard, K. A. Bertness, T. E. Harvey, L. M. Mansfield, A. W. Sanders, N. A. Sanford, *IEEE Trans. Nanotechnol.* **2008**, *7*, 760.
[150] P. T. Blanchard, K. A. Bertness, T. E. Harvey, A. W. Sanders, N. A. Sanford, S. M. George, D. Seghete, *IEEE Trans. Nanotechnol.* **2012**, *11*, 479.
[151] Ž. Gačević, D. López-Romero, T. J. Mangas, E. Calleja, *Appl. Phys. Lett.* **2016**, *108*, 033101.
[152] Y. Jo, D. Son, D. Lee, C. Won, J. H. Seo, I. M. Kang, J. Lee, presented at *2015 73rd Annual Device Research Conference (DRC)*, Columbus, OH June **2015**.
[153] F. Yu, D. Rümmler, J. Hartmann, L. Caccamo, T. Schimpke, M. Strassburg, A. E. Gad, A. Bakin, H.-H. Wehmann, B. Witzigmann, H. S. Wasisto, A. Waag, *Appl. Phys. Lett.* **2016**, *108*, 213503.
[154] F. Yu, S. Yao, F. Römer, B. Witzigmann, T. Schimpke, M. Strassburg, A. Bakin, H. W. Schumacher, E. Peiner, H. S. Wasisto, A. Waag, *Nanotechnology* **2017**, *28*, 095206.
[155] Z. Hu, W. Li, K. Nomoto, M. Zhu, X. Gao, M. Pilla, D. Jena, H. G. Xing, presented at *2017 75th Annual Device Research Conference (DRC)*, South Bend, IN June **2017**.
[156] F. Yu, K. Strempel, M. F. Fatahilah, H. Zhou, F. Römer, A. Bakin, B. Witzigmann, H. W. Schumacher, H. S. Wasisto, A. Waag, *IEEE Trans. Electron Dev.* **2018**, *65*, 2439.
[157] A. Chaney, H. Turski, K. Nomoto, Q. Wang, Z. Hu, M. Kim, H. G. Xing, D. Jena, presented at *2018 76th Device Research Conf. (DRC)*, Santa Barbara, June **2018**.
[158] D.-H. Son, Y.-W. Jo, J. H. Seo, C.-H. Won, K.-S. Im, Y. S. Lee, H. S. Jang, D.-H. Kim, I. M. Kang, J.-H. Lee, *Solid-State Electron.* **2018**, *145*, 1.

[159] A. Lundskog, C.-W. Hsu, K. Fredrik Karlsson, S. Amloy, D. Nilsson, U. Forsberg, P. Olof Holtz, E. Janzén, *Light Sci. Appl.* **2014**, *3*, e139.
[160] M. J. Holmes, K. Choi, S. Kako, M. Arita, Y. Arakawa, *Nano Lett.* **2014**, *14*, 982.
[161] X. Sun, P. Wang, B. Sheng, T. Wang, Z. Chen, K. Gao, M. Li, J. Zhang, W. Ge, Y. Arakawa, B. Shen, M. Holmes, X. Wang, *Quantum Eng.* **2019**, *100*, e20.
[162] M. Holmes, S. Kako, K. Choi, M. Arita, Y. Arakawa, *Phys. Rev. B* **2015**, *92*, 115447.
[163] T. J. Puchtler, T. Wang, C. X. Ren, F. Tang, R. A. Oliver, R. A. Taylor, T. Zhu, *Nano Lett.* **2016**, *16*, 7779.
[164] P. Dimitrakis, P. Normand, C. Bonafos, E. Papadomanolaki, E. Iliopoulos, *Appl. Phys. Lett.* **2013**, *102*, 053117.
[165] A. Aiello, Y. Wu, A. Pandey, P. Wang, W. Lee, D. Bayerl, N. Sanders, Z. Deng, J. Gim, K. Sun, R. Hovden, E. Kioupakis, Z. Mi, P. Bhattacharya, *Nano Lett.* **2019**, *19*, 7852.
[166] Y. Wu, X. Liu, P. Wang, D. A. Laleyan, K. Sun, Y. Sun, C. Ahn, M. Kira, E. Kioupakis, Z. Mi, *Appl. Phys. Lett.* **2020**, *116*, 013101.